Materials Chemistry and Physics

Structural, optical and magnetic properties of stencil-free printed ZnO layers doped with Fe^{2+} and Fe^{3+} ions

G.S. Pekar *, A.F. Singaevsky, O.Y. Kolomys, V.V. Strelchuk, P.M. Lytvyn

HIGHLIGHTS

- Polycrystalline layers of ZnO doped with Fe2+and Fe3+ ions are manufactured by a method of stencil-free printing developed.
- The printed Fe-doped ZnO layers exhibit ferromagnetic behavior at room temperature.
- The value of magnetization in the ZnO:Fe3+ layers is twice that in the printed layers of ZnO:Fe2+, ZnO:Co2+ and ZnO:Mn2+.
- A simple and cheap method for stencil-free printing of DMS layers is promising for fabricating the spintronics elements.

ARTICLE INFO

Keywords:
$Fe^{2+}$and Fe^{3+} doped ZnO
Printed polycrystalline layers
Uniform distribution of Fe ions In the Zn sites
Magnetization at room temperature

ABSTRACT

In this paper we investigate the doping effect of FeO and Fe_2O_3 on the structural, optical and magnetic properties of ZnO layers prepared by a new stencil-free technique. Samples were characterized by X-ray diffraction (XRD), atom force and magnetic force microscopy, photoluminescence and Raman spectroscopy. A quite high quality of the printed Fe-doped ZnO layers was demonstrated. It was shown that the incorporated Fe^{2+} or Fe^{3+} ions substitute Zn^{2+} ions in ZnO lattice and, unlike the doped layers prepared by other technological methods, were uniformly distributed in the Zn^{2+} sites. The levels of doping with different impurities that make it possible to obtain layers free of second phase inclusions were established. The printed ZnO:Fe layers illustrated pronounced ferromagnetic behavior at ambient conditions. The values of the magnetic field correlated with the impurity content. The value of magnetization of the ZnO:Fe^{3+} layers was shown to be approximately twice that of the printed ZnO:Fe^{2+} layers. At the same time, magnetization of ZnO:Fe^{2+} layers was approximately the same as of the printed ZnO:Co^{2+} and ZnO:Mn^{2+} layers studied by us previously. The higher magnetization observed in ZnO:Fe^{3+} layers was supposed to be due to the carrier-mediated mechanism of magnetization in these layers.

1. Introduction

The future development of electronics, which should lead, in particular, to a significant increase in the productivity of computer technology, is often considered to be associated with a new branch of electronics called spintronics. Unlike conventional electronics, spintronics makes it possible to control not only the charge of an electron but also its spin. In other words, it becomes possible to use two degrees of freedom of an electron, connected with its charge and spin. As it was shown, such a mechanism can be implemented in solid solutions of the magnetic d-transition metals in diamagnetic semiconductors which are called diluted magnetic semiconductors (DMS).

Over the past two decades, DMS studies have been carried out quite widely, they have been reflected in more than 2000 experimental and theoretical articles as well as in some reviews, among which we would like to highlight the papers by T. Dietl et al. [1] and by Straumal et al. [2]. In particular, it was concluded that zinc oxide doped with Co, Mn, or Fe may serve as a very promising DMS material. It was also found that ferromagnetism appeared in the polycrystalline layers or films (but not in single crystals) and the grain boundaries were responsible for the ZnO ferromagnetic behavior. Moreover, not only a high specific density of grain boundaries (i.e. their quantity) was important but also the structure of grain boundaries, as well as the distribution of boundaries over the orientations and misorientations. Since all these requirements are, in fact, very general, it remains to be hoped that at least some of the developed technologies for the manufacture of zinc oxide will satisfy

these very vague requirements. With more or less success, the potentially ferromagnetic ZnO layers and films were prepared by a great variety of technological techniques including the liquid ceramics method, powder sintering, wet chemistry, chemical vapor deposition, plasma-assisted molecular-beam epitaxy, radio-frequency magnetron sputtering, ion implantation, pulsed laser deposition, etc. The ferromagnetic behavior at the highest temperatures (up to 800 K) was observed in ZnO thin films grown by plasma-assisted molecular-beam epitaxy and implanted with Co ions [3]. However, quite often the results on fabrication DMS with ferromagnetic properties were poorly reproducible and the nature of ferromagnetism remained uncertain. It often turned out that the ferromagnetism observed was due to secondary phase formation what made the material unsuitable for use in spintronics. All this makes it necessary to look for new methods and modes of DMS manufacturing.

In our investigations, we manufacture the ZnO-based DMS using printing methods. To date, printing technologies are not widely used in modern electronics despite they are quite simple, cheap, and may be easily integrated into industrial semiconductor technologies.

In our previous research the technology of stencil-free printing developed by us [4] was applied for manufacturing, for the first time, the printed ZnO:Co layers which exhibit ferromagnetism at room temperature [5]. In the present work, the printed layers of ZnO doped with Fe^{2+} and Fe^{3+} ions were manufactured and studied and the peculiar features of those layers were established. Those studies were aimed at:

- to work out a technique for printing ZnO layers doped with iron;
- to find out the conditions for the incorporation of iron ions into the lattice of printed ZnO layers and to establish the position of those ions in ZnO lattice;
- to study the structure, luminescence, and magnetic properties of ZnO layers and reveal the differences in these properties when doped with ferrous and ferric ions;
- to establish the conditions under which doping with iron does not lead to the formation of the second-phase inclusions in the ZnO lattice;
- to establish the differences in the effect of doping with Fe^{2+} and Fe^{3+} ions on the magnetization of printed ZnO:Fe layers;
- to obtain the printed ZnO:Fe layers reproducibly characterized by the presence of ferromagnetism and to compare its value with the value of ferromagnetism in the printed ZnO layers doped with other magnetic metals.

2. Materials and stencil-free method for printing Fe doped ZnO layers

2.1. Chemicals

To manufacture the paste, we used ZnO powder from Sigma-Aldrich with a purity of 99.999%, as well as FeO, Fe_2O_3, propylene glycol and boric acid produced in Ukraine, with a purity of 99.5%.

2.2. Preparation

The ZnO layers studied in this work were prepared by printing. Usually, when talking about printed layers of semiconductor materials, one means layers made by screen printing [6–8]. When using that method, the paste which contains the printed material is applied to the mesh stencil and then the paste is pushed through the cells of the stencil on the substrate surface. And, finally, the layers are recrystallized at high temperature.

Unlike the widespread liquid ink printing, the screen printed layers of semiconductors may be defective due to the higher density and heterogeneity of the pastes containing the semiconductor materials. The voids formed in the crossing points of the wires forming the mesh serve as sources of air bubbles that passed to the wet paste when applied. As a result, the semiconductor layers, after their recrystallization, could contain pores and other damages. In addition, mesh cells could be clogged with paste, and despite cleaning the cells, they could contain residues of dried paste which contaminated the prepared semiconductor layers and impaired their quality.

The improved printing method proposed by us [4,5] is free from the above disadvantages. As distinct from the screen-printing method, we did not use stencils and placed the paste directly on the surface of the (0001)-sapphire substrate. In order to adjust the layer thickness, the substrate was supplied by two parallel guides fixed on the opposite edges of the substrate. Those guides were thin wires, fibers, or tapes with a thickness of 25–50 μm. The paste used to prepare ZnO layers contained ZnO powder, boric acid powder which served as a flux (catalyst), and propylene glycol which served as a binder. In addition, the bivalent or trivalent iron ions were introduced into the paste by adding the calculated amount of the fine powder of FeO or Fe_2O_3, respectively.

After applying the paste to the surface of the substrate, a scraper was moved along the substrate surface in a direction parallel to the guides. The scraper removed the paste layer above the guides and the remaining layer was of the same thickness as the thickness of the guides. Then we removed the guides from the substrate, after which the printed wet layer of the paste was dried and then recrystallized at a temperature 1000-1100 °C for 1.5–2.0 h in a quasi-closed volume which impedes the evaporation of the layer material and ensures the stability of the chemical composition of the semiconductor layer.

The steps of the process of layer fabrication are shown in the diagram 1.

The Fe-doped ZnO layers obtained were polycrystalline, strong, continuous, and densely packed. The thickness of the layers after drying and recrystallization was usually less than their initial thickness. The thickness of the layers could be changed by using the guides of various thicknesses but mainly we manufactured the layers with a thickness of about 25 μm.

The quality of the obtained layers was assessed using an optical microscope at 600x magnification. As a rule, no obvious defects (such as bubbles, cracks, pores, foreign inclusions, bulges) were observed. The adhesion of the layer to the substrate was assessed by scribing with a diamond tool. It turned out to be good over the entire surface of the layers.

As for the physical properties of the fabricated layers, we first of all note that they exhibited pronounced semiconducting properties, in particular, photosensitivity. For example, the resistivity of ZnO:Fe^{2+} layers with iron content about 5% decreased from $8 \cdot 10^4$ Ohm•cm in the dark to $6 \cdot 10^3$ Ohm•cm under standard illumination of 1.5 a.m. The similar results were obtained for ZnO:Fe^{3+} layers with the same iron content, however, their resistivity both in the dark and under standard illumination was about twice lower as compared with ZnO:Fe^{2+} layers.

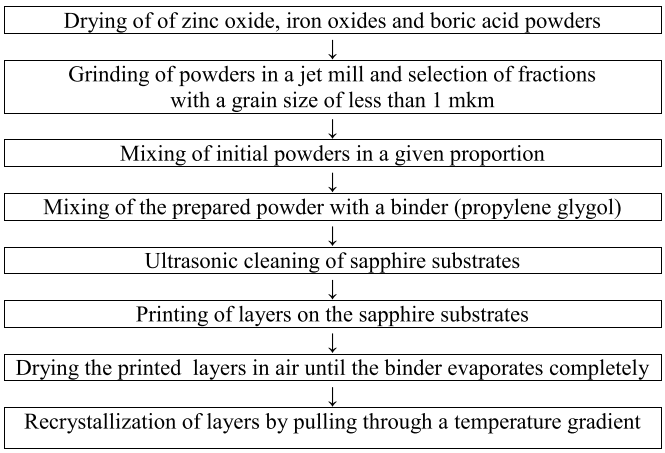

Diagram 1. Scheme of layer fabrication.

It is obvious that we could not be sure in advance that the layers printed by the described method would possess ferromagnetism. It was shown previously [1] that for the manifestation of ferromagnetism the samples should not only be polycrystalline but also be characterized by a sufficiently high density of grain boundaries and have a required structure of amorphous intercrystalline layers. However, these requirements were only of a general nature and were not quantified, so the way to implement them remained undefined.

2.3. Characterization

Characterization by XRD and Raman spectroscopy was used to analyze the changes in the structural and vibrational features due to the doping which may contribute to the lattice site distortion or a secondary phase formation [9,10].

The structure and composition of the stencil-free printed Fe-doped ZnO layers were characterized by powder X-ray diffraction (XRD). Diffraction patterns we obtained with automatic powder diffractometer Shimadzu LabX XRD-6000 ($Cu_{K\alpha}$-radiation, $\lambda = 0{,}154178$ nm).

The Raman and photoluminescence measurements were carried in backscattering configuration using Horiba Jobin-Yvon T64000 triple spectrometer with integrated Olympus BX41 microscope. The Raman spectra were excited using the 488-nm line of an Ar/Kr laser. The laser beam was focused on the sample surface into the spot of about 0.5 μm in diameter. The laser power on the sample surface was always kept below 2 mW to avoid laser-induced damage. Low-temperature photoluminescence (PL) spectra were excited using the 325-nm line of a He–Cd laser. Taking the absorption coefficient (α) of ZnO to be 1.6×10^5 cm^{-1} at 325 nm ($h\nu = 3.81$ eV) [9], the characteristic penetration depth ($1/\alpha$) of excitation wavelength (325 nm) comes out to be about 60 nm. So the observed PL emission is restricted within few tens of nanometer from the upper surface of the sample.

As for the possible change in the properties of layers under the influence of about 2 mW power, we had the proof that no significant heating of the layers occurred. It was the invariability of the position of the phonon mode (E_2^{high}) and invariability of the ratio of the intensities of phonon mode (E_2^{high}) in the Stokes and anti-Stokes Raman spectra.

Topography and local magnetic properties of the crystalline surface features were characterized by atomic and magnetic force microscopy (AFM, MFM). Measurements were performed at ambient conditions using NanoScope IIIa Dimension 3000™ scanning probe microscope.

The two-pass MFM technique was applied to eliminate relief influence on MFM data. The lift height of 800 nm was used. Hard magnetic probes with a coercivity of about 300 Oe (the NANOSENSORS™ PPP-MFMR probe) were used. MFM tips were magnetized before measurements along the tip axis in the magnetic field of the permanent magnet. For better identification of the surface features exhibiting magnetic properties, the surface areas were sequentially mapped with an MFM probe magnetized in opposite directions (north and south poles at tip apex). Since the investigated layers contained sometimes an electrostatic charge, all samples were discharged prior to the MFM measurements.

Relative magnetizations of ZnO:FeO and ZnO:Fe_2O_3 layers was estimated through force-distance measurements of magnetic interactions.

3. Results and discussion

3.1. X-ray diffraction analysis

The crystal structure of undoped and doped with FeO and Fe_2O_3 ZnO layers were studied using powder X-ray diffractometry. The analysis of the XRD diffraction patterns (Fig. 1) has shown that all synthesized samples with different doping contents gave several intense and narrow XRD peaks represent various crystallite orientations showing that layers are polycrystalline nature. The angular position of XRD peaks is well matched with the Joint Committee Powder Diffraction Standards card (JCPDS 036–1451) of the hexagonal ZnO wurtzite polycrystalline structure (random distribution of crystallite orientations) [11].

In the XRD patterns of the undoped (Fig. 1, curve 1) and Fe doped ZnO layers with Fe concentration up to 5 at% (Fig. 1 a,b), curves 2,3) ZnO layers had no XRD peaks corresponding to any secondary phases of Fe. Thus, Fe^{2+} (Fe^{3+}) ions exhibit a solid solubility up to 5 at % in the host ZnO lattice. The broadening and the shift of peaks in the XRD pattern confirm the preferential incorporation of Fe ions into the ZnO lattice [12]. However, in the case of 5 at% of Fe^{2+} (Fe^{3+}) ions (Fig. 1 a,b, curve 4), XRD patterns clearly showed the main phase of hexagonal ZnO (JCPDS No. 36–1451) superimposed to a minor secondary phase of Fe_3O_4 (Fe_2O_3) (JCPDS No. 65–3107).

It can be expected that at higher doping levels some portion of the added Fe^{2+}(Fe^{3+}) ions will be insoluble and segregate at the grain boundaries so that Fe_3O_4 or Fe_2O_3 will be formed. Recently it was shown that with the increase in doping level of Fe_2O_3 in ZnO, the secondary phase was formed at the grain boundaries, which seemed to inhibit the ZnO grain size growth due to pinning effect [13].

The X-ray diffraction pattern of the undoped ZnO layers showed the

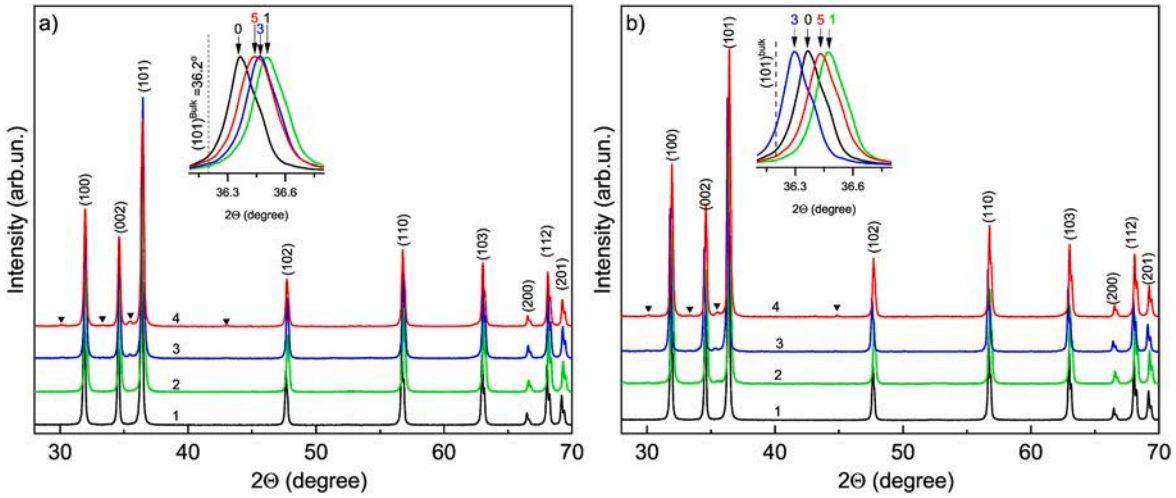

Fig. 1. X-ray patterns of undoped ZnO (curve 1), ZnO:FeO (a) and ZnO:Fe_2O_3 (b) layers with Fe concentration of 1 at.% (curve 2), 3 at.% (curve 3) and 5 at.% (curve 4). The characteristic XRD peaks attributed to the secondary phase Fe_3O_4 (Fe_2O_3) are marked symbols ▼. The inset shows the magnified view of the (101) diffraction peaks.

most intense diffraction peak (101) at 36.37°, which was shifted towards larger angles compared to bulk ZnO crystal (36.2°) due to the lattice mismatch (about 18%) between the ZnO layer and sapphire substrate [14]. The small width (0.18–0.20^0) of all XRD peaks indicated a sufficiently high quality of the ZnO crystal structure [15]. As compared with the undoped ZnO layers, both types of Fe doped ZnO layers showed a decrease in the intensity and an increase in the half-width of the XRD peaks. For 1 at % Fe^{2+}-doped ZnO:FeO layers, a sharp shift of the (101) peak towards larger angles up to 36.51° was observed. At the same time, an increase in the concentration from 1 to 5 at% of Fe^{3+} ions in ZnO:Fe_2O_3 layers led to a gradual shift of the (101) peak towards smaller angles (see Table 1). This behavior (101) of the peak position could be associated with different ionic radii of Fe ions when they replaced Zn^{2+} ions in ZnO matrix [16]. Thus, when Fe ions were introduced in the ZnO lattice, it underwent contraction or expansion depending on the ionic radii of the dopant. To explain these phenomena, note that the ionic radius of Fe^{2+}, Zn^{2+}, and Fe^{3+} ions are equal to 0.78 Å, 0.76 Å, and 0.64 Å, respectively [17]. Therefore, a sharp shift of the (101) peak at Fe^{3+} concentration of 1% was due to significant compression deformations resulted from the substitution of Zn^{2+} ions by Fe^{3+} ions. In this case, oxygen ions O^{2-} will be directed to Fe^{3+} ions to maintain the balance of charge [18,19]. In the case of ZnO doping with FeO, the value of the shift of the (101) peak towards small angles was due to the replacement of Zn^{2+} ions by Fe^{2+} ions whose sizes were close to each other [20]. In the case of ZnO doping with Fe_2O_3, the nonmonotonic shift of the (101) diffraction peak reflected the different charge states of Fe^{3+} and Zn^{2+} ions. In this case, the concentration of zinc ions decreased to compensate for the charge, which inhibited the growth of ZnO crystallites and crystal quality reduces.

To determine the effect of iron ions on the structural parameters of ZnO polycrystalline layers, some characteristic values were determined, in particular, the crystallite size D, lattice parameters (a, c, c/a), and strain. The results of the calculations are presented in Table 1.

It should be noted that the XRD spectra of ZnO:FeO (Fig. 2a) and ZnO:Fe_2O_3 (Fig. 2b) include the low-intensity diffraction peaks that do not belong to the XRD peaks of ZnO. For example, the XRD peaks noted in Fig. 2 by a symbol ▼ recorded at 30.1°, 35.5°, 43.1°, and 53.5° correspond to the crystal planes (220), (311), (400), (422) and (511) of the mixed oxide FeO + Fe_2O_3 which has a spinel structure (according to JCPDSNo. 65–3107 [21]). Usually it is written as Fe_3O_4 or Fe_2O_3 [22,23]. In our case the presence of Fe_3O_4 complicates the situation similarly to the case described in Ref. [24].

3.2. Micro-Raman studies

Studies of Raman scattering in the doped ZnO layers were carried out to obtain information about the change in crystal structure and the local lattice distortions that can be caused by doping, The aim of the Raman studies of the ZnO:FeO and ZnO:Fe_2O_3 layers was also to compare the effects of distortions of the crystalline structure in ZnO doped with Fe^{2+} and Fe^{3+} ions having different ionic radii as well as the establishing the existence of the secondary phases under the doping used.

Fig. 2 shows the Raman spectra of undoped and doped with different concentrations of the FeO (i.e. Fe^{2+} ions) (a) and Fe_2O_3 (i.e. Fe^{3+} ions) (b) ZnO layers in the range from 90 to 800 cm^{-1}. In undoped ZnO layers, we have observed the strong narrow bands at about 98 cm^{-1} ($\Gamma \sim 1.6$ cm^{-1}) and 437 cm^{-1} ($\Gamma \sim 5.0$ cm^{-1}) corresponding E_2^{low} and E_2^{high} phonon modes of ZnO, respectively. With increasing Fe concentration, the E_2^{high} phonon band is high-frequency shifted at about 0.6 cm^{-1} as compared to the position of E_2^{high} phonon mode in the unstrained ZnO layers (437.0 cm^{-1}) due to elastic compressive strain in the plane of the layer growth [25]. At the same time, the intensity of the E_2^{low} phonon band is decreased and is shifted from 98.5 to 98.2 cm^{-1} for ZnO:FeO and to 98.1 cm^{-1} for ZnO:Fe_2O_3. The observed weak bands at 378 cm^{-1} and 412 cm^{-1} correspond to A_1(TO) and E_1(TO) modes of ZnO. In the Raman spectra of the ZnO:FeO and ZnO:Fe_2O_3 layers (Fig. 2), the increasing of Fe content in ZnO up to 5 at.% leads to the decrease of intensity and broadening of E_2^{high} and E_2^{low} phonon bands, possibly due to the breaking of translational symmetry caused by intrinsic defects and/or by doping with Fe. In addition, with increasing of Fe content in ZnO:FeO layers from 1 to 5 at.%, the position of the maximum of E_2^{high} band (see the insert in Fig. 3a) is downshifted from 437.1 cm^{-1} to 435 cm^{-1}, while in ZnO:Fe_2O_3 layers a downshift from 437.2 cm^{-1} to 436.4 cm^{-1} occurs (Fig. 3b). This effect may be due to strain-induced change in the binding energy of Zn–O resulted from the replacement of Zn^{2+} ions by Fe^{2+} ions whose ionic radius (0.78 Å) is larger that the ionic radius of Fe^{3+} ions (0.64 Å) [17]. Thus, Raman measurements show a direct correlation between strain-induced frequency shift of E_2^{high} phonon mode due to differences in ionic radii of Fe^{2+} and Fe^{3+} ions.

In the Raman spectra of undoped ZnO layers, a wide $A(E)_1(LO)$ band is observed at 584 cm^{-1} which corresponds to the superposition of both LO (A_1 and E_1) vibrational ZnO modes. The increase of this band, the intensity of which is usually small due to the processes of destructive interference between the mechanisms of Fröhlich interaction and the deformation potential in the scattering process on LO phonons in ZnO, is due to distortion of translational symmetry connected with the intrinsic and impurity structural defects [26]. The introduction of Fe^{2+} (Fe^{3+}) ions into the ZnO lattice leads to a low-frequency shift of the $A(E)_1(LO)$ band from 585 to 578 cm^{-1} which may be due to a decrease in the misorientation of crystallites from the c axis ([0001] direction). It was also observed that the introduction of the iron ions and/or the new structural defects lead to the violation of the translational symmetry and the increase in the intensity of the complex-shape vibrational bands in the frequency range of 500–750 cm^{-1} [27]. Futhermore, the second-order Raman bands were also observed which were due to multi-phonon processes such as overtone of 2TA mode at 204 cm^{-1}, E_2^{high} -E_2^{low} mode at 331,7 cm^{-1}, 2LA ($2B_1^{low}$)(Γ,M) mode at 539 cm^{-1}, TA + TO(H,M) and TA + LO(L,H) at 618 and 653 cm^{-1} (Fig. 2a, inset), respectively [28].

It should be noted that in the Raman spectra of all ZnO:Fe_2O_3 layers (Fig. 3b), the additional (new) phonon bands at 289, 462 and 507 cm^{-1} were observed which corresponded to E_g, $T_{2g}(2)$, and $T_{2g}(3)$ symmetry phonon modes of Fe_3O_4 [29,30]. In addition, we observed the increase of intensity of these bands with increasing Fe_2O_3 contamination.

Table 1
The structural parameters of undoped, FeO-doped, and Fe_2O_3-doped ZnO layers.

Dopant conc., at.%	2θ (101), deg.	$(I_{doped})/I_{undoped})$ (101), %	FWHM, deg.	D (101), nm	a, nm	c, nm	c/a	Strain, × 10^{-3}
0	36.378	100	0.183	45	0.3240	0.5192	1.602	2.43
ZnO:FeO								
1	36.514	95	0.193	43	0.3227	0.5173	1.603	2.55
3	36.474	90	0.206	40	0.3231	0.5178	1.603	2.73
5	36.450	79	0.222	37	0.3233	0.5182	1.603	2.94
ZnO:Fe_2O_3								
1	36.483	86	0.191	43	0.3230	0.5177	1.603	2.53
3	36.307	79	0.178	46	0.3248	0.5202	1.602	2.37
5	36.442	44	0.219	38	0.3234	0.5183	1.603	2.90

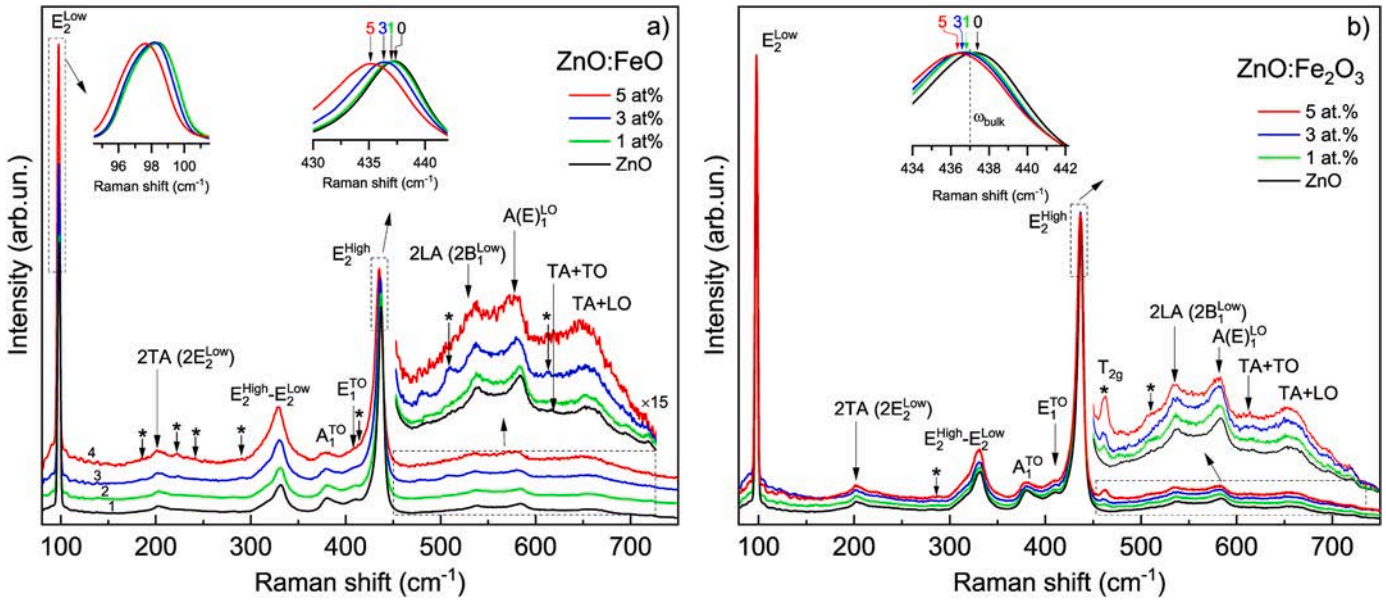

Fig. 2. Micro-Raman spectra of undoped ZnO (curve 1), ZnO:FeO (a) and ZnO:Fe_2O_3 (b) layers with Fe concentration of 1 at.% (curve 2), 3 at.% (curve 3) and 5 at.% (curve 4). The inserts show the frequency positions of E_2^{low} and E_2^{high} phonon modes in ZnO layers with different Fe concentrations. All spectra are vertically shifted for clarity and normalized to E_2^{high} bands maxima.

Supposing that the Raman band at 462 cm^{-1} arised from the vibrations of the AO_4 tetrahedral groups, the increase in the intensity and high wave numbers shift could be a direct consequence of the replacement of Zn atoms by lighter Fe atoms [31]. These bands were not observed in ZnO:FeO layers (Fig. 3a). At the same time, under dopant concentration from 3 to 5%, the weak additional bands at 185, 224, 245, 291, 413, 480, 503 and 613 cm^{-1} were observed in the Raman spectra of ZnO:FeO layers. These bands were not observed both in undoped and Fe_2O_3-doped ZnO layers and correspond to α-Fe_2O_3 (hematite) ($A_{1g}(1)$ ~224 cm^{-1}, $E_g(1)$ ~ 245 cm^{-1}, $E_g(2)$ ~ 292 cm^{-1}, $E_g(3)$ ~ 413 cm^{-1}, $E_g(4)$ ~ 613 cm^{-1}) [32,33]. The bands at 480 and 503 cm^{-1} may be due to maghemite γ-Fe_2O_3 [30]. The appearance of the small amount of the secondary phases was found at more than 5.0 at% of Fe which may be explained by reaching the threshold of thermodynamic solubility limit of Fe ions in ZnO layers.

3.3. Photoluminescence

As known, photoluminescence (PL) spectroscopy is a very sensitive tool to study impurities and defects in semiconductors. Fig. 3 presents the low-temperature normalized PL spectra of ZnO layers doped with FeO and Fe_2O_3 at nominal Fe concentrations 1, 3, and 5 at.%. The PL spectra of the ZnO layers include the near-band edge (NBE) excitonic emission in the UV region (at 380 nm) and green-centered broad band commonly related to deep-level defects (called also the deep-level emission (DLE) bands). The NBE emission consists of several sharp emission bands due to free excitons, donor-bound excitons, donor-acceptor pair (DAP) transitions, and their longitudinal-optical (LO) phonon replicas with an energy separation of 72 meV. In the visible green-yellow spectral region DLE bands were observed which were attributed to the intrinsic structural defects like zinc interstitials (Zn_i) or oxygen vacancies (V_O) as donor defects and zinc vacancies (V_{Zn}) or oxygen interstitials (O_i) as acceptor defects [34].

Fig. 3 presents the PL spectra of the undoped and Fe-doped ZnO layers. It can be seen that all samples exhibited a strong NBE luminescence with a DLE band in the visible spectral range. The NBE luminescence corresponds to the radiative recombination of free excitons (FX) and bound excitons (BX) on neutral donor (D^0X) and acceptor (A^0X) [35,36]. Furthermore, the PL spectra of all samples, shown in Fig. 3, contain the same features and resemble each other which can be understood in terms of the similar crystalline structure of the layers studied.

With increasing Fe concentration, the ratio between the integrated spectral intensity of NBE and DLE bands decreases indicating an increase in the contribution of recombination due to defect levels. The intensity of the DLE luminescence band of the doped samples increases with increasing Fe concentration up to 5 at.%. At the same time, in Fe-doped layers the intensity of the NBE band decreases by about 10 times. Such a quenching of luminescence can be explained by the fact that the photogenerated electrons preferentially occupy the Fe ion induced trap centers [17,38]. The D^0X band is commonly assigned to interstitial hydrogen donor-bound excitons with an activation energy of 0.046 eV [37,38].

Note that in all samples studied the FX emission band at 3.366 eV and D^0X band at 3.352 eV were observed (inset in Fig. 3a and b) which is indicative of the perfect crystalline structure of the printed layers studied.

By studying the PL spectra (inset in Fig. 3 a,b) we have found that, with the increase of doping concentration, the D^0X та FX emission bands exhibit a blue shift in optical band gap up to 3.356 eV for ZnO:FeO and 3.358 eV for ZnO:Fe_2O_3. This blue shift of the exciton emission bands can be explained on the basis of the increase in elastic deformations due to incorporated iron because the Fe^{2+} and Fe^{3+}ions have the ionic radii of 0.78 Å and 0.645 Å respectively, which is nearly 5% more and 12% less than that of the Zn^{2+} ion. Thus, the doping in ZnO with Fe is expected to produce the varying bond length of Zn^{2+}-O^{2-} (1.947 Å), Fe^{2+}-O^{2-} (2.155 Å), and Fe^{3+}-O^{2-} (2.012 Å) due to the substitution of multivalent Fe ions at the Zn sites.

The absorption edge blue shifts with increasing iron content in ZnO nanoparticles was observed previously [39] and was explained in terms of the Burstein-Moss band filling effect (BM shift). With the partial substitution of Fe^{3+} ions at the Zn^{2+} sites in the heavily doped samples, the concentration of free electrons is increased and the states at the bottom of the conduction band are filled (the Fermi level of the host n-type ZnO has moved into the conduction band) resulting in an increase in the bandgap.

The strong intensity of the emission band at 3.33 eV is caused by the radiative recombination of free electrons from the conduction band to the holes bound to an acceptor state (FA) [40,41] which can be located

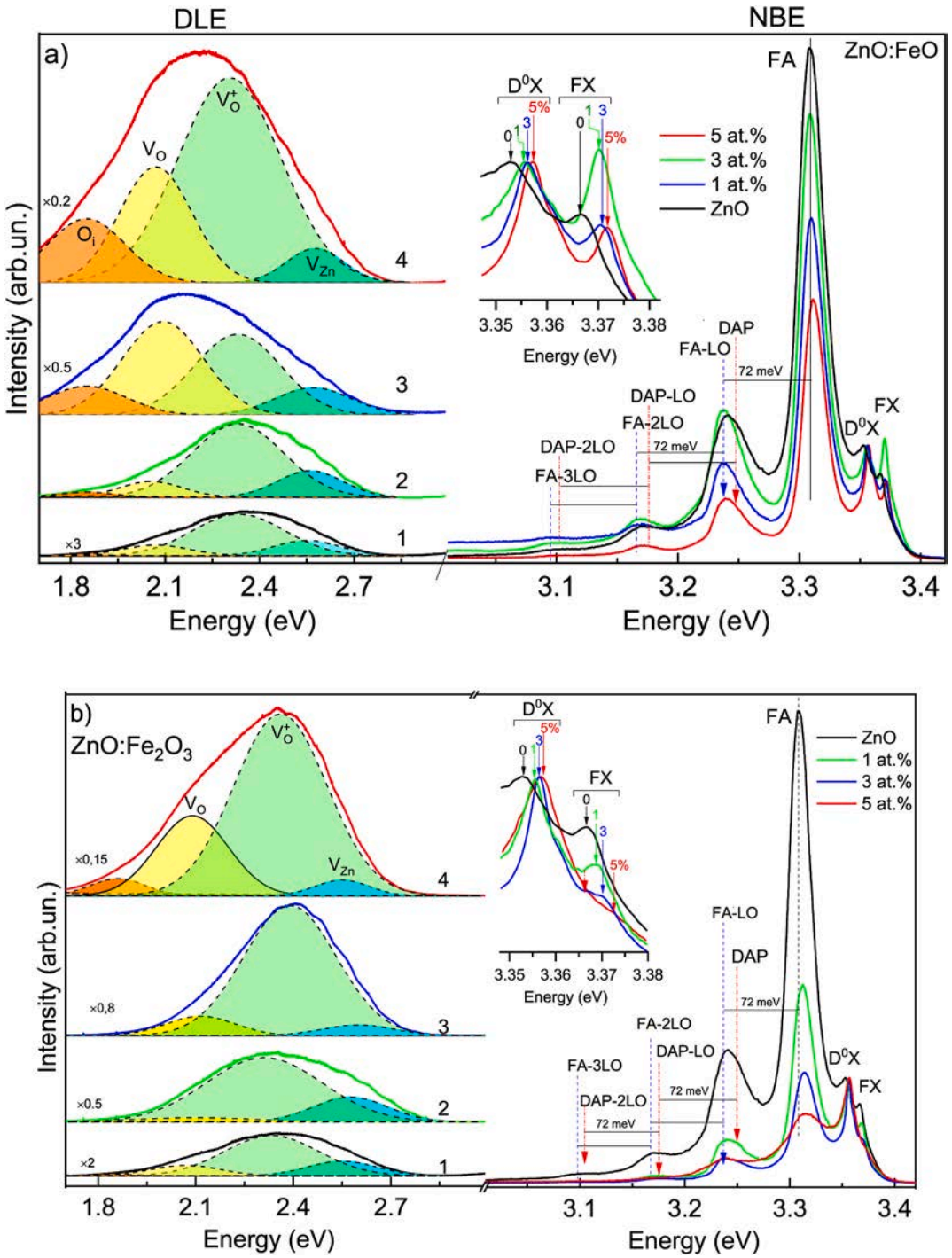

Fig. 3. Low-temperature PL spectra of undoped ZnO (curve 1), ZnO:FeO (a) and ZnO:Fe_2O_3 (b) layers with Fe concentration of 1 at.% (curve 2), 3 at.% (curve 3) and 5 at.% (curve 4). T = 77 K, E_{exc} = 3.81 eV (λ_{exc} = 325 nm). The DLE bands are shifted vertically for a better visualization.

in the near-surface region of microcrystals ZnO [42]. The corresponding phonon replicas are marked in Fig. 3. The 3.236 eV donor–acceptor-pair emission (the high-energy wing of the FA-LO band) is the indicator of the presence of shallow acceptor levels.

In undoped ZnO layers, the weak structured DLE band assigned to transitions involving a shallow donor and a deep acceptor was observed. It may be noted that we did not observed intraionic emission of the Fe dopant as reported in Ref. [43]. The DLE of the undoped ZnO layers is deconvoluted into four Gaussian peaks centered at about 2.56, 2.36, 2.07 and 1.87 eV, which were marked to the blue, green, yellow and orange colors respectively to show their relative differences (Fig. 3a and b). The luminescence band at about 2.56 eV is typically assigned to acceptor Zinc vacancy V_{Zn}or Zn_i - V_{Zn} [44,45]. The green and yellow bands around 2.33 eV and 2.1 eV were assigned to singly ionized (V_O^+) and neutral oxygen vacancy (V_O) [46,47]. The orange band at 1.87 eV was attributed to oxygen interstitials (O_i), which act as traps for photo-generated holes [48]. A deconvolution analysis of the DLE was done for the ZnO:FeO and ZnO:Fe_2O_3 layers with different iron concentrations. With increasing Fe concentration, we observed not only DLE shift towards the yellow part of the spectrum but also an overall increase of DLE as compared with a weak DLE intensities in the undoped layers. Note that, for all DLE bands, the contributions of oxygen vacancies

prevailed and the well-known green-yellow luminescence was observed. In the samples doped up to 3 at.% Fe, the intensity of the band related to defects was decreased whereas the intensity of the bands due to V_O and O_i defects was increased. Therefore, it may be supposed that Fe^{3+} and $Fe^{/2+}$ ions can be incorporation into the sites of zinc vacancies. When the Zn^{2+} ions are replaced with Fe^{3+} ions, the oxygen ions would be drawn to the Fe^{3+} ions to keep the balance of charge [49,50]. Herewith the interstitial oxygen (O_i) should be formed and the distribution of oxygen became imbalanced. In our case this effect was revealed in an increase in the intensity of green-yellow and orange DLE bands.

3.4. Surface morphology and magnetic properties of ZnO layers doped with Fe^{2+} (Fe^{3+}) ions

The local magnetic properties of ZnO layers with different contents of magnetic impurities were studied by the method of magnetic force microscopy (MFM). The result of the measurements is a map of the magnetic stray field gradient over the surface of the sample quantified by the shift of the oscillation frequency of the magnetic probe (Fig. 4). MFM measurements demonstrated the peculiarities of the formation of the magnetic microstructure in ZnO:FeO and ZnO:Fe_2O_3 layers with variations in the concentration of magnetic impurities in the range of 1–5 at.%. At room temperature, the magnetic microstructure was a characteristic superposition of the layer grain field. There was a general correlation of MFM maps with a macrorelief of the surface (i.e. fluctuations of layer thickness) and some single grains present a strong magnetic contrast in Fe-doped layers (Fig. 4 b,d).

The increase in the impurity content resulted in the increase of the stationary magnetic stray field above the surface of the sample, which was manifested in the form of lines of the light-dark contrast and lower sensitivity to the fluctuation of the layer's thickness. Individual grains in the layer were more pronounced over the MFM map, had a high level of magnetization, and could be of a different polarity (arrow marked in Fig. 4,d). Note, that no local contrast was detected that could be associated with segregations/clusters of the iron impurities. As the content of the magnetic impurity increased, there was a tendency to decrease the grain size of the layers (for ZnO:FeO from 500 nm to 280 nm).

The values of magnetization of the layers with different Fe contamination were evaluated by the macro-force magnetic interaction of the layers with the applied external magnetic field (Table 2). By studying the dependences of the strength of the magnetic interaction on the layer-magnet distance, relative values of magnetization were measured. For ease of comparison, the values of magnetizations were normalized to the

Table 2
Relative magnetization of ZnO:FeO and ZnO:Fe_2O_3 layers.

Fe content in the layers, at.%	Magnetization in ZnO:Fe_2O_3, %	Magnetization in ZnO:FeO, %
1	14.5	9.8
3	61.0	44.2
5	100.0	77.5

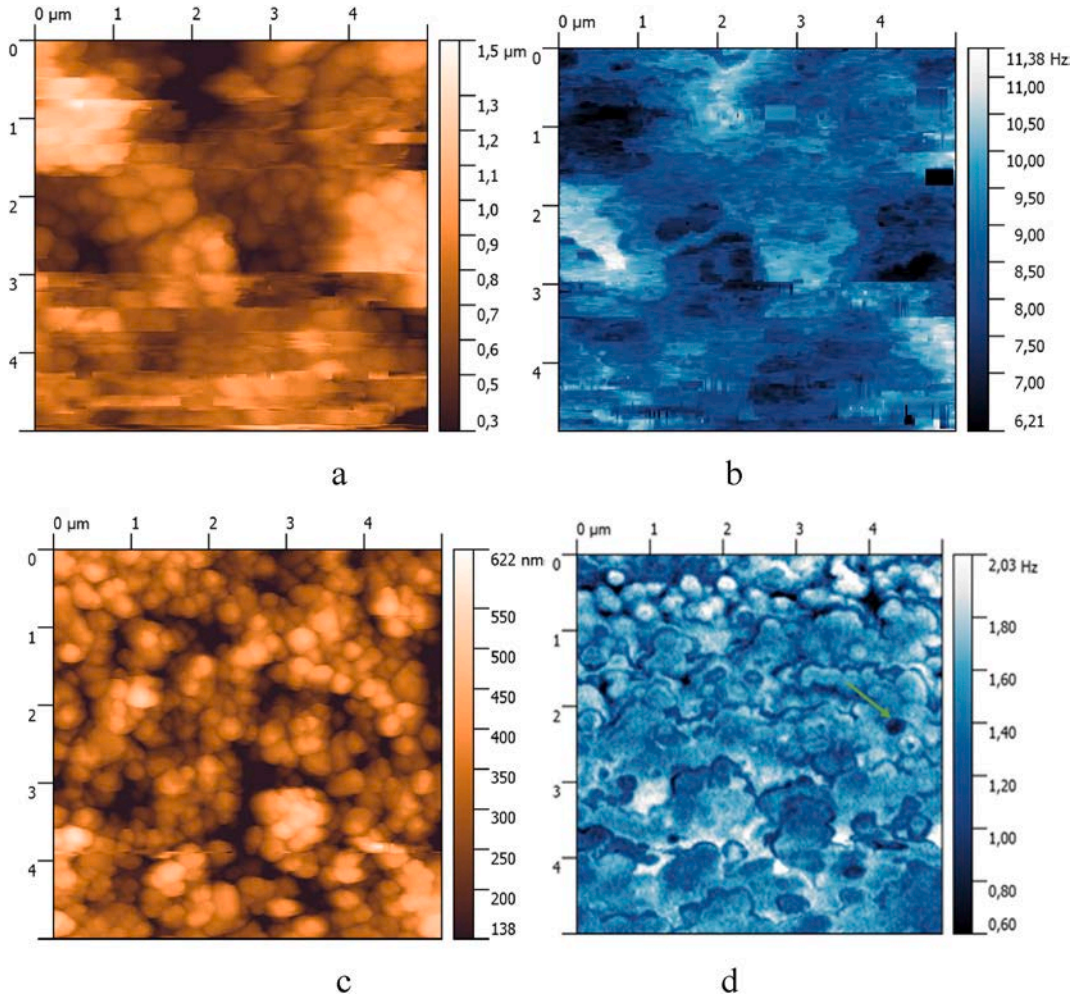

Fig. 4. Topography maps (left) and magnetic field gradient (right) in ZnO layers with an iron content of 1 at. % (a, b) and 5 at .% (c, d). Arrow marks the single grain of opposite polarity.

maximum inherent in the sample ZnO:Fe_2O_3 (at 5 at.% of Fe).

The fact that the magnetization of the layers increases when the layers are doped with trivalent rather than divalent ions is not unexpected. This effect was previously observed in ZnO films doped with Co^{2+} and Co^{3+} ions and was explained by fact that the incorporated trivalent ion may supply the third ("extra") electron of the outer shell to the conduction band of the host semiconductor. It results in the increase of conductivity of the doped layer and promotes the carrier mediated mechanism of magnetization [3,51].

As regards the comparison of the magnetization of ZnO layers with different dopants, it should be noted that the value of magnetization of the layers doped with Fe_2O_3 exceeded the magnetization not only of the layers doped with FeO but also of the ZnO:Co [5] and ZnO:Mn layers printed by us by the same method as ZnO:Fe layers studied in the present work. The magnetization of the layers ZnO:Co and ZnO:Mn was approximately the same as that of the layers doped with FeO.

We managed also to prepare inclusions-free ZnO layers with Fe contamination of about 10%. Their magnetization was found to be higher than at lower iron concentrations, and these layers were even attracted to a magnet brought to their surface. This could serve as one more proof of the ferromagnetism of the layers.

4. Conclusions

The layers of a diluted magnetic semiconductor (DMS), namely ZnO doped with di- and trivalent Fe ions were fabricated for the first time by a new stencil-free technique. This technique was shown to make it possible to obtain layers free of pores and other damages. To study the layer properties, the methods of scanning electron microscopy, energy-dispersive X-ray spectroscopy, atom force microscopy, magnetic force microscopy as well as the methods for studying the optical absorption, the low-temperature photoluminescence, and Raman scattering, were jointly applied. As a result. the effect of doping on the structural, optical, recombination, and other properties of the layers, as well as on the width of their bandgap, the size of the crystal cell, etc, was established.

It was found that the prepared layers had a densely packed and rather uniform polycrystalline wurtzite structure with a typical grain size of about 550 nm. The lattice parameters were slightly changed by impurity incorporation without changing the ratio of lattice parameters c/a. It was shown that during doping, Fe^{2+} or Fe^{3+} ions substituted Zn^{2+} ions in the ZnO lattice and were uniformly distributed in the Zn^{2+} sites of the lattice, unlike the doped ZnO layers and films prepared by other technological methods and described in the literature.

It was shown that printed ZnO:Fe layers illustrate pronounced ferromagnetic behavior at ambient conditions. The values of the magnetic field correlated with the impurity content. The levels of doping with different impurities that make it possible to obtain layers free of second phase inclusions were established. It was shown, in particular, that although the fluctuations of a magnetic field value over the layer surface were observed, those fluctuations were caused by long-range self-consistent magnetic interactions between grains but not by a clustering of the dopants.

And, finally, it turned out that the value of magnetization of the ZnO:Fe^{3+} layers was approximately twice that of the printed ZnO:Fe^{2+} layers. At the same time, magnetization of ZnO:Fe^{2+} layers was approximately the same as of the printed ZnO:Co^{2+} and ZnO:Mn^{2+} layers studied by us previously. The higher magnetization observed in ZnO:Fe^{3+} layers can be attributed to the carrier-mediated mechanism of magnetization in these layers.

The fact that the ferromagnetic properties were inherent in ZnO layers doped with all magnetic impurities used and these properties were always fully reproducible showed that the method of printing developed is suitable for generating these properties. If we accept that, according to Ref. [2], some peculiar features of the DMS polycrystalline structure (such as the structure of the grain boundaries, their orientation and disorientation, the specific area of grain boundaries per unit volume, etc.) are decisive factors in the formation of ferromagnetic properties, we may assume that such structural features are inherent in the printed ZnO layers fabricated by the stencil-free method used in this work.

Declaration of competing interest

The authors declare that they have no known competing financial interests or personal relationships that could have appeared to influence the work reported in this paper.

References

[1] T. Dietl, H. Ohno, F. Matsukura, J. Cibert, D. Ferrand, Zener model description of ferromagnetism in zinc-blende, Magnetic Semiconductors Science 287 (2000) 1019–1022. https://doi:10.1126/science.287.5455.1019.

[2] B.B. Straumal, S.G. Protasova, A.A. Mazilkin, G. Schütz, E. Goering, B. Baretzky, P. B. Straumal, Ferromagnetism of zinc oxide nanograined films, JETP Lett. (Engl. Transl.) 97 (2013) 367–377, https://doi.org/10.1134/S0021364013060143.

[3] Z. Yang, M. Biasini, W.P. Beyermann, M.B. Katz, O.K. Ezekoye, X.Q. Pan, Y. Pu, J. Shi, Z. Zuo, J.L. Liu, Electron carrier concentration dependent magnetization and transport properties in ZnO:Co diluted magnetic semiconductor thin films, J. Appl. Phys. 104 (2008), https://doi.org/10.1063/1.3033402, 113712-1–113712-7.

[4] N.M. Osipyonok, G.S. Pekar, A.F. Singaevsky, Method of Applying Solid Layers by Screen Printing Method, 10.05.2011. Patent for invention of Ukraine No. 94561.

[5] G.S. Pekar, A.F. Singaevsky, O.F. Kolomys, V.V. Strelchuk, P.M. Lytvyn, M. M. Osipyonok, I.A. Vasin, M.A. Skoryk, Magnetic and optical properties of printed ZnO:Co polycrystalline layers, Mater. Sci. Semicond. Process. (2021) (in print).

[6] N. Suyama, T. Arita, Y. Nishiyama, N. Ueno, S. Kitamura, M. Murozono, Screen-printed CdS/CdTe solar cells, Optoelectron. - Devices Technol. 5 (1990) 259–274, https://doi.org/10.1016/0379-6787(84)90100-5.

[7] V.P. Klad'ko, O.S. Lytvyn, P.M. Lytvyn, N.M. Osipenok, G.S. Pekar, I. V. Prokopenko, A.F. Singaevsky, A.A. Korchevoy, Recrystallization processes in screen-printed CdS films, Semiconductor Physics, Quantum Electronics andOptoelectronics 5 (2002) 170–175. https://doi:dspace.nbuv.gov.ua/handle/123456789/121180.

[8] V.P. Klad'ko, P.M. Lytvyn, N.M. Osipyonok, G.S. Pekar, I.V. Prokopenko, A. F. Singaevsky, Screen-printed p-CdTe layers for CdS/CdTe solar cells, Semiconductor Physics, Quantum Electronics and Optoelectronics 8 (2005) 61–65. https://doi:dspace.nbuv.gov.ua/handle/123456789/121646.

[9] V. Strelchuk, O. Kolomys, S. Rarata, P. Lytvyn, O. Khyzhun, Chan oeurn chey, omer nur and magnus willander Raman submicron spatial mapping of individual Mn-doped ZnO nanorods, Nanoscale Research Letters 12 (2017) 351, https://doi.org/10.1186/s11671-017-2127-4.

[10] V.V. Strelchuk, A.S. Nikolenko, O.F. Kolomys, S.V. Rarata, K.A. Avramenko, P. M. Lytvyn, P. Tronc, Chan Oeurn Chey, Omer Nur, Magnus Willander Optical and structural properties of Mn-doped ZnO nanorods grown by aqueous chemical growth for spintronic applications, Thin Solid Films 601 (2016) 22–27, https://doi.org/10.1016/j.tsf.2015.11.019.

[11] American Society for Testing and Material, Powder Diffraction Files, Joint Committee on Powder Diffraction Standards: Swarthmore, PA, 1999, 3-888.

[12] R. Djenadic, G. Akgül, K. Attenkofer, M. Winterer, Chemical Vapor Synthesis and Structural Characterization of nanocrystalline Zn1−xCoxO (x=0-0.50) particles by X-ray diffraction and X-ray absorption spectroscopy, J. Phys. Chem. C 114 (2010) 9207–9215, https://doi.org/10.1021/jp908148y.

[13] Zhijian Peng, Xiuli Fu, Yanxu Zang, Zhiqiang Fu, ChengbiaoWang, Longhao Qi, Hezhuo Miao, Influence of Fe_2O_3 doping on microstructural and electrical properties of ZnO– Pr_6O_{11} based varistor ceramic materials, J. Alloys Compd. 508 (2) (2010) 494–499, https://doi.org/10.1016/j.jallcom.2010.08.100.

[14] V. Srikant, J.S. Speck, D.R. Clarke, Mosaic structure in epitaxial thin films having large lattice mismatch, J. Appl. Phys. 82 (1997) 4286–4295, https://doi.org/10.1063/1.366235.

[15] V. Mote, Y. Purushotham, B. Dole, Williamson-Hall analysis in estimation of lattice strain in nanometer-sized ZnO particles, J Theor Appl Phys 6 (2012) 6, https://doi.org/10.1186/2251-7235-6-6.

[16] A. Abdel-Baset, Yue-Wen Fang, B. Anis, Chun-Gang Duan, M. Abdel-Hafiez, Structural and magnetic properties of transition-metal-doped Zn1−xFexO, Nanoscale Res. Lett. 11 (2016) 115, https://doi.org/10.1186/s11671-016-1332-x.

[17] R.D. Shannon, Revised effective ionic radii and systematic studies of interatomic distances in halides and chalcogenides, Acta Cryst.Acta Cryst. A32 (1976) 751–767, https://doi.org/10.1107/S0567739476001551.
[18] W. Cheng, X. Ma, Structural, optical and magnetic properties of Fe-doped ZnO, J. Phys.: Conf, Ser 152 9 (2009), 012039, https://doi.org/10.1088/1742-6596/152/1/012039, 2009.
[19] Y. Zhang, L. Wu L, H. Li, J. Xu, L. Han, B. Wang, Z. Tuo, E. Xie, Influence of Fe doping on the optical property of ZnO films, J. Alloys Compd. 473 (2009) 319–322, https://doi.org/10.1016/j.jallcom.2008.05.090.
[20] N.M. Ba-Abbad, A.A.H. Kadhum, A.B. Mohamad, M.S. Takriff, K. Sopian, Visible light photocatalytic activity of Fe^{3+}-doped ZnO nanoparticle prepared via sol–gel technique, Chemosphere 91 (11) (2013) 1604–1611. https://doi:10.1016/j.chemosphere.2012.12.055.
[21] C. Yu, D. Zhang, X. Dong, Q. Lin, Pyrolytic behavior of a zero-valent iron biocharcomposite and its Cu(II) removal mechanism, RSC Adv. 8 (2018) 34151–34160, https://doi.org/10.1039/C8RA05676E.
[22] Alvaro Ruíz-Baltazar, Esparza Rodrigo, Gerardo Rosas, Ramiro Pérez, Effect of the surfactant on the growth and oxidation of iron nanoparticles, J. Nanomater. 2015 (2015), https://doi.org/10.1155/2015/240948. Article ID 240948, 8 pages.
[23] W. Kim, C.-Y. Suh, S.-W. Cho, et al., A new method for the identification and quantification of magnetite-maghemite mixture using conventional X-ray diffraction technique, Talanta 94 (2012) 348–352.
[24] E.A. Campos, D.V. Pinto, J.I.S. Oliveira, E.C. Mattos, R.C.L. Dutra, Synthesis, characterization and applications of iron oxide nanoparticles, J. Aero. Technol. Manag. 7 (3) (2015), https://doi.org/10.5028/jatm.v7i3.471.
[25] X. Wei, Y. Zhao, Z. Dong, J. Li, Investigation of native defects and property of bulk ZnO single crystal grown by a closed chemical vapor transport method, J. Cryst. Growth 310 (2008) 639–645, https://doi.org/10.1016/j.jcrysgro.2007.10.080.
[26] A. Sayari, A. Marzouki, A. Lusson, M. Oueslati, V. Sallet, Annealing and partial pressure ratio effects on ZnO films grown by metal-organic chemical vapor deposition using tert- butanol as oxidant, Thin Solid Films 518 (2010) 6870–6875, https://doi.org/10.1016/j.tsf.2010.07.031.
[27] A.K. Pradhan, K. Zhang, G.B. Loutts, U.N. Roy, Y. Cui, A. Burger, Structural and spectroscopic characteristics of ZnO and ZnO:Er3+ nanostructures, J. Phys. Condens. Matter 16 (2004) 7123–7129. https://doi:10.1088/0953-8984/16/39/043.
[28] R. Cuscó, E. Alarcón-Lladó, J. Ibáñez, L. Artús, J. Jiménez, B. Wang, M. Callahan, Temperature dependence of Raman scattering in ZnO, Phys. Rev. B 75 (2007) 165202, https://doi.org/10.1103/PhysRevB.75.165202.
[29] I. Chourpa, L. Douziech-Eyrolles, L. Ngaboni-Okassa, J.-F. Fouquenet, S. Cohen-Jonathan, M. Soucé, H. Marchais, P. Dubois, Molecular composition of iron oxide nanoparticles, precursors for magnetic drug targeting, as characterized by confocal Raman microspectroscopy, Analyst130 (2005) 1395–1403, https://doi.org/10.1039/B419004A.
[30] O.N. Shebanova, P. Lazor, Raman spectroscopic study of magnetite ($FeFe_2O_4$): a new assignment for the vibrational spectrumJ, Solid State Chem 174 (2003) 424–430, https://doi.org/10.1016/S0022-4596(03)00294-9.
[31] A. Manohar, C. Krishnamoorthi, K.C.B. Naidu, C. Pavithra, Dielectric, magnetic hyperthermia, and photocatalytic properties of ZnFe2O4 nanoparticles synthesized bysolvothermal reflux method, Appl. Phys. A 125 (7) (2019) 477–486. https://doi:10.1007/s00339-019-2760-0.
[32] P. Kumar, V. Sharma, J.P. Singh, A. Kumar, S. Chahal, K. Sachdev, K.H. Chae, A. Kumar, K. Asokan, D. Kanjilal, Investigations on Magnetic and Electrical Properties of Zn doped Fe2O3 Nanoparticles and their correlation with local electronic structure, J. Magn. Magn Mater. 489 (2019) 165398, https://doi.org/10.1016/j.jmmm.2019.165398.
[33] M. Aaron, Jubb, heather C. Allen vibrational spectroscopic characterization of hematite, maghemite, and magnetite thin films produced by vapor deposition, ACS Appl. Mater. Interfaces 2 (10) (2010) 2804–2812, https://doi.org/10.1021/am1004943.
[34] K. Vanheusden, C.H. Seager, W.L. Warren, D.R. Tallant, J.A Voigt, Correlation between photoluminescence and oxygen vacancies in ZnO phosphors Appl, Phys. Lett. 68 (1996) 403, https://doi.org/10.1063/1.116699.
[35] X. Guo, C.P. Tripp, C. Chen, Y. Wang, S. Yin, W. Qin, Temperature dependence of the photoluminescence from ZnO microrods prepared by a float zone method, CrystEngComm 18 (2016) 3130–3135, https://doi.org/10.1039/C6CE00349D.
[36] H. Morkoç, Ü. Özgür, Zinc Oxide: Fundamentals, Materials and Device Technology, John Wiley & Sons, Hoboken, NJ, USA, 2009. ISBN 9783527408139.
[37] B.K. Mayer, H. Alvies, D.M. Hofmann, W. Kriegseis, D. Forster, F. Bertraim, J. Christen, A. Hoffmann, M. Straburg, M. Dworzak, U. Haboeck, A.V. Rodina, Phys. Status Solidi B 241 (2004) 231–260, https://doi.org/10.1002/pssb.200301962.
[38] D.K. Hwang, H.S. Kim, J.H. Lim, J.Y. Oh, J.H. Yang, S.J. Park, K.K. Kim, D.C. Look, Y.S. Park, Appl. Phys. Lett. 86 (2005) 151917, https://doi.org/10.1063/1.1895480.
[39] Anindita Samanta, M.N. Goswami, P.K. Mahapatra, Fe-doped ZnO nanoparticles as novel photonic and multiferroic semiconductor, Mater. Chem. Phys. 240 (2020) 122180, https://doi.org/10.1016/j.matchemphys.2019.122180.
[40] N. Maharjan, R.C. Rai, D.D. Mulmi, M.L. Nakarmi, Observation of band gap renormalization in mesoscopic zinc oxide particles, J. Lumin. 219 (2020) 116879–116883. https://doi:10.1016/j.jlumin.2019.116879.
[41] D.-K. Hwang, H.-S. Kim, J.-H. Lim, J.-Y. Oh, J.-H. Yang, S.-J. Park, K.K. Kim, D. C. Look, Y.S. Park, Study of the photoluminescence of phosphorus-doped p-type ZnO thin films grown by radio-frequency magnetron sputtering, Appl. Phys.Letts 86 (2005), 151917- 1 –151917-3, https://doi:10.1063/1.1895480.
[42] V.S. Yalishev, Y.S. Kim, X.L. Deng, B.H. Park, S.U. Yuldashev, Study of the photoluminescence emission line at 3.33 eV in ZnO films, J. Appl. Phys. 112 (2012), 013528, https://doi.org/10.1063/1.4733952.
[43] Nanotechnology 20 (2009) 135704. http://iopscience.iop.org/0957-4484/20/13/135704.
[44] T. Moe Børseth, B.G. Svensson, A. Yu, Kuznetsov. dentification of oxygen and zinc vacancy optical signals in ZnO, Appl. Phys. Lett. 89 (2006) 262112, https://doi.org/10.1063/1.2424641.
[45] E.G. Barbagiovanni, R. Reitano, G. Franzò, V. Strano, A. Terrasia, S. Mirabella, Radiative mechanism and surface modification of four visible deep level defect states in ZnO nanorods, Nanoscale 8 (2016) 995–1006, https://doi.org/10.1039/C5NR05122C.
[46] M.J. Al-Saadi, S.H. Al-Harthi, H.H. Kyaw, et al., Influence of atomic hydrogen, band bending, and defects in the top few nanometers of hydrothermally prepared zinc oxide nanorods, Nanoscale Res Lett 12 (2017) 22, https://doi.org/10.1186/s11671-016-1800-3.
[47] S. Dellis, N. Pliatsikas, N. Kalfagiannis, et al., Broadband luminescence in defect-engineered electrochemically produced porous Si/ZnO nanostructures, Sci. Rep. 8 (2018) 6988, https://doi.org/10.1038/s41598-018-24684-6.
[48] E.G. Barbagiovanni, et al., Universal model for defect-related visible luminescence in ZnO nanorods, RSC Adv. 6 (2016) 73170–73175.
[49] W. Cheng, X. Ma, Structural, optical and magnetic properties of Fe-doped ZnO, J Phys Conf Ser 152 (2009), 012039, https://doi.org/10.1088/1742-6596/152/1/012039.
[50] Y. Zhang, L. Wu, H. Li, J. Xu, L. Han, B. Wang, Z. Tuo, E. Xie, Influence of Fe doping on the optical property of ZnO films, J. Alloys Compd. 473 (2009) 319, https://doi.org/10.1016/j.jallcom.2008.05.090.
[51] G. Lashkarev, V. Karpyna, V. Dobrowolski, V. Lazorenko, V. Baturin, A. Karpenko, R. Szymczak, M. Baran, W. Pacuski, Electronic states of cobalt in ZnO:Co films, Ukrainian J. Phys. 51 (2006) 493–496. http://archive.ujp.bitp.kiev.ua/files/journals/51/5/510510p.pdf.